

Optimal and robust error filtration for quantum information processing

Aaqib Ali,^{1,2} Giovanni Scala,^{3,2} and Cosmo Lupu^{3,1,2}

¹*Dipartimento Interateneo di Fisica, Università di Bari, 70126 Bari, Italy*

²*INFN, Sezione di Bari, 70126 Bari, Italy*

³*Dipartimento Interateneo di Fisica, Politecnico di Bari, 70126 Bari, Italy*

Error filtration is a hardware scheme that mitigates noise by exploiting auxiliary qubits and entangling gates. Although both signal and ancillas are subject to local noise, constructive interference (and in some cases post-selection) allows us to reduce the noise level in the signal qubit. Here we determine the optimal entangling unitary gates that make the qubits interfere most effectively, starting from a set of universal gates and proceeding by optimizing suitable functionals by gradient descent or stochastic approximation. We examine how our optimized scheme behaves under imperfect implementation, where ancillary qubits may be noisy or subject to cross-talk. Even with these imperfections, we find that adding more ancillary qubits helps in protecting quantum information. We benchmark our approach against figures of merit that correspond to different applications, including entanglement fidelity, quantum Fisher information (for applications in quantum sensing), and CHSH value (for cryptographic applications), with one, two, and three ancillary qubits. With one and two ancillas we also provide analytical explicit expressions from an ansatz for the optimal unitary. We also compare our method with the recently introduced Superposed Quantum Error Mitigation (SQEM) scheme based on superposition of causal orders, and show that, for a wide range of noise strengths, our approach may outperform SQEM in terms of effectiveness and robustness.

I. INTRODUCTION

Quantum information science has opened the door to revolutionary advancements in computing [1–3], sensing [4–6], and communication [7, 8], but one of the biggest hurdles remains maintaining quantum coherence. As we navigate the Noisy Intermediate-Scale Quantum (NISQ) era [9], suppressing and mitigating the effects of noise and errors in quantum systems is critical [10–16]. In this work, we investigate and develop schemes of *error filtration*, a method introduced by Gisin, Linden, Maszar, and Popescu [17] to filter noise and purify entanglement. Here we first formulate error filtration in a most general framework and then optimize specific filtration strategies to achieve optimal performance in a variety of applications within quantum information processing. In this way, we propose error reduction schemes that advance the most effective solution currently available in the literature, enhancing the reliability and accuracy of quantum operations, where large-scale fault-tolerant architectures are not yet feasible [18]. We believe that our optimized scheme provides a useful tool in the portfolio of techniques [17, 19], giving users the flexibility to choose the best option based on their accuracy needs and the amount of overhead they are willing to accept.

Figure 1 illustrates a rather general scheme of error filtration. An input state $|\psi\rangle$ is subject to a memoryless noisy channel, denoted \mathcal{E} , modeling storage in a quantum memory or transmission through an optical fiber — both of which degrade information and introduce errors. To protect the quantum information in $|\psi\rangle$ from these errors, error filtration introduces n auxiliary systems initially prepared in $|0\rangle^{\otimes n}$, which are coupled to the signal via an encoding (and entangling) unitary U . When retrieving the information, either from a quantum memory or after transmission through the fiber, the decoding pro-

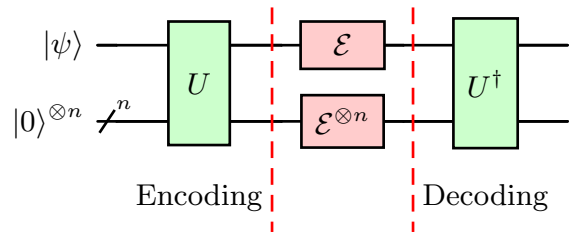


FIG. 1: General scheme of error filtration. On the left, one signal qubit $|\psi\rangle$, and n ancillary qubits $|0\rangle^{\otimes n}$. After the encoding U on the signal and ancillae, the information is transmitted through a *local* noisy channel \mathcal{E} . The inverse unitary U^\dagger is applied for the decoding before the reading process (in some cases the signal is retrieved with post-selection on the ancillas.).

cess is performed by applying the inverse of the unitary transformation before reading the data.

The challenge we address here is to determine the *optimal* unitary acting on $N = n + 1$ qubits given a noise model, a task that is computationally demanding due to the exponential growth of the $2^{2N} - 1$ parameters in $SU(2^N)$. Nevertheless, it is possible to find the optimal encoding unitary that protects information despite the noise acting on the ancillary qubits. Furthermore, we show that error filtration remains effective even in the presence of preparation noise in the auxiliary qubits and cross-talk among the signal and the ancillas. Finally, our numerical results suggest an analytical ansatz for the optimal unitary, eliminating computational time. This is useful for applications like Quantum Key Distribution, where prolonged computations would hinder efficiency and the ability to make real-time adjustments.

Our filtration scheme is optimized according to spe-

cific figures of merit, determined by the particular goal achieved through quantum information processing.

Depending on them, we consider also the post-selected state of the signal qubit conditioned on a measurement of the ancillas. For computation and general quantum information processing, we focus on the entanglement fidelity [20]. The CHSH functional is considered as a theoretical tool to study non-locality and for implementing device-independent protocols [21–25]. Finally, for metrology and sensing applications we examined the quantum Fisher information [26].

Unlike other works based on variational methods, see e.g. [27], or focused on specific subclasses of encoding unitaries [28–33], our optimization scheme, although computationally demanding, is ansatz-free as we aim at finding the globally optimal encoding and decoding unitaries. Remarkably, through optimization over universal $U \in SU(2^N)$ gates, our work generalizes and encompasses previous results [28–30] that focused on specific encodings.

Showing the success of our implementation is the first stage to propose experimental robust error reduction strategies, even in the presence of noise and cross-talk in the pre- and post-processing operations. We investigate systems with up to three auxiliary qubits, providing practical solutions for error reduction in photonic (e.g. for adapting multicore fibers to quantum communication) and for the characterization of quantum memories [34, 35], each corresponding to a different figure of merit [36–38].

The paper proceeds as follows. In Section II we introduce a suitable parameterization for the encoding and decoding unitary, and the noise model. The numerical optimization results, and an ansatz for the optimal encoding, are presented in Section III. In particular, the robustness of error filtration under imperfect implementation is discussed in Section III D. A comparison with the SQEM approach of Ref. [28] is presented in Section IV. Conclusions and an overview of future development are presented in Section V.

II. ERROR FILTRATION FROM UNIVERSAL UNITARY GATES

In this section, we define an error-free encoding unitary U (see Fig. 1) to encode the signal qubit with the support of n auxiliary qubits initially prepared in $|0\rangle$. All the $N = n + 1$ qubits are sent through a memoryless noisy channel \mathcal{E} as described in Sec. II B.

A. Universal unitary gates

We use universal unitary gates for their ability to approximate any quantum operation, enabling a wide range of applications.

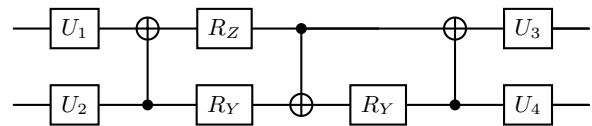


FIG. 2: Construction of a two-qubit unitary gate from four single-qubit gates $U_1, U_2, U_3, U_4 \in SU(2)$, three CNOT gates, two rotations along the y -axis, and one along the z -axis [39].

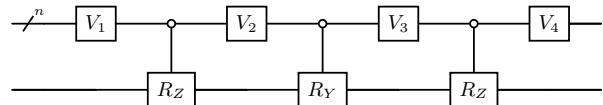


FIG. 3: Quantum Shannon Decomposition for constructing $U \in U(2^{n+1})$ involving recursive application of $V_1, V_2, V_3, V_4 \in U(2^n)$ and multiplexed rotations [50]. The recursive definition of the multiplexed rotation is shown in Fig. 4.

The literature offers multiple decomposition strategies, including Givens rotations and sine-cosine decompositions, which provide a structured methodology for simplifying complex quantum gates into more manageable subunits (see Refs. [40–49]).

For the specific task of constructing a two-qubit unitary transformation (i.e. for an error filtration scheme with $n = 1$ ancillary qubit), we adopt the circuit architecture described in Ref. [39]. Figure 2 illustrates how a generic two-qubit unitary gate $U \in U(2^2)$ can be synthesized from single-qubit gates and the two-qubit gate CNOT, where $R_X = e^{-i\theta\sigma_x/2}$, $R_Y = e^{-i\phi\sigma_y/2}$, and $R_Z = e^{-i\gamma\sigma_z/2}$, where $\sigma_x, \sigma_y, \sigma_z$ are the Pauli matrices. (These can be combined following Euler decomposition to obtain general one-qubit unitaries.)

To expand this construction to more qubits (number of ancillas $n \geq 2$), we employ the Quantum Shannon Decomposition (QSD) described in Ref. [50]. The QSD method recursively allows for the implementation of an arbitrary $(n + 1)$ -qubit unitary operation through a sequence of multiplexed rotations and n -qubit unitaries, arranged in a specific circuit configuration as depicted in Figs. 3–5. However, while the QSD recursion is adaptable to circuits with any number of qubits, it does increase the number of required C-NOT gates. This trade-off is managed by recursively applying the decomposition until the circuit simplifies to two-qubit gates, after which we use minimal decomposition [50].

With this decomposition, we control 15, 72, and 312 parameters respectively for U acting on one signal qubit and $n = 1, 2, 3$ ancillae. Note that these numbers exceed $2^{2N} - 1$ free parameters of $SU(2^N)$. The cost we paid to have a more suitable decomposition for the experiments we aim to simulate and propose.

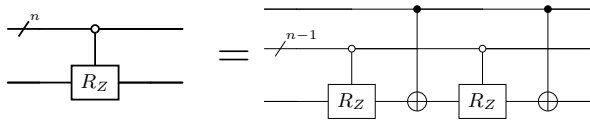


FIG. 4: By recursively applying the decomposition shown in the picture, one can decompose any multiplexed rotation into elementary gates [50].

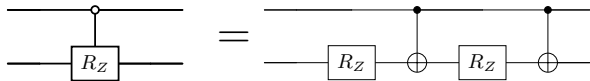


FIG. 5: For $n = 1$, the multiplexed rotation is defined by combining two C-NOT gates and two single-qubit rotations. Note that in general the two single-qubit rotations have different angles [50].

B. Noise models

In the error filtration circuit depicted in Fig. 1 we assume a consistent noisy channel affecting both signal and ancillary qubits. As an example, we explore two prevalent models of quantum noise: the *dephasing channel* and the *depolarizing channel*. In the following, we recall their action in a Bell state $|\psi\rangle$. The dephasing channel, denoted as \mathcal{E}_φ , affects the relative phase between $|0\rangle$ and $|1\rangle$ in the following Kraus representation:

$$\{\sqrt{p_\varphi} \sigma_0, \sqrt{1-p_\varphi} \sigma_z\}, \quad (1)$$

where σ_0 denotes the identity matrix. The action of this channel on the Bell state preserves the states in the computational basis states but introduces phase errors:

$$\mathcal{E}_\varphi(|\psi\rangle\langle\psi|) = q_\varphi |\psi\rangle\langle\psi| + (1-q_\varphi) \tau_\psi, \quad (2)$$

where $q_\varphi = 2p_\varphi - 1$ and

$$\tau_\psi = \frac{|\psi\rangle\langle\psi| + \sigma_z |\psi\rangle\langle\psi| \sigma_z}{2} \quad (3)$$

is the state with erased phase information. The depolarizing channel, denoted as \mathcal{E}_r , models the loss of quantum information without bias towards any specific basis. Its effect on a quantum state can be described using the Kraus operators:

$$\left\{ \sqrt{p_r} \sigma_0, \sqrt{\frac{1-p_r}{3}} \sigma_x, \sqrt{\frac{1-p_r}{3}} \sigma_y, \sqrt{\frac{1-p_r}{3}} \sigma_z \right\}. \quad (4)$$

The channel transforms any input state towards the maximally mixed state $\sigma_0/2$. The action on a pure state $|\psi\rangle$ is

$$\mathcal{E}_r(|\psi\rangle\langle\psi|) = q_r |\psi\rangle\langle\psi| + (1-q_r) \frac{\sigma_0}{2}, \quad (5)$$

where the parameter $q_r = (4p_r - 1)/3$ quantifies the probability that the input state remains unchanged, and $(1-q_r)$ is the probability that it is replaced by the maximally mixed state.

III. NUMERICAL RESULTS AND THEORETICAL INSIGHTS

In this section, we denote by \mathfrak{F} , a generic cost function, such as entanglement fidelity, the CHSH functional, or quantum Fisher information, which acts on the output state ρ_U^{out} from the circuit in Fig. 1. We explicitly remark the dependence of the state ρ_U^{out} on the unitary $U \in \text{SU}(2^{n+1})$ that encodes the initial state made of an input signal qubit $|\psi\rangle$ and ancillary qubits initialized in $|0\rangle$. The optimal value of \mathfrak{F}_n^* is given by

$$\mathfrak{F}_n^* = \max_{U \in \text{SU}(2^{n+1})} \mathfrak{F}[\rho_U^{\text{out}}]. \quad (6)$$

As the number of ancillae increases, the functional improves since $\text{SU}(2^{n+1})$ is a subgroup of $\text{SU}(2^{n+2})$, leading to $\mathfrak{F}_{n+1} \geq \mathfrak{F}_n \geq \mathfrak{F}_0$, where $n = 0$ represents no error reduction. However, in practice, larger circuits introduce more noisy gates, limiting the *theoretical* benefits of error reduction via coherent wavefunction interference.

The robustness of the optimal filtration scheme to the noise arising from the preparation of the auxiliary qubit, and from cross-talk between different qubits, is discussed in Section III D.

A. Optimization scheme

As discussed in Section II A, circuits with $n = 1, 2, 3$ ancillas require 15, 72, and 312 parameters, respectively. While optimization with one ancilla is straightforward, the exponential increase in parameters with additional ancillas requires substantial computational resources. To address this, we utilized the ReCaS-Bari Data Center [51], a high-performance computing (HPC) cluster with 8000 cores capable of running parallel jobs. Circuit optimization was performed using *PennyLane*, a Python library tailored for machine learning techniques suited to large parameter spaces¹.

For optimization, the best results were achieved using both gradient descent and gradient-free optimizers, with convergence monitored to determine the number of iterations. Multiple runs with different random seeds ensured stability and consistency. This approach enhances the performance and reliability of quantum circuits.

B. Entanglement fidelity

For systems with non-ergodic and non-stationary transmission, such as fibres very sensible to temperature perturbations, a time-dependent window must be characterized to dynamically adjust U in real-time. In

¹ Code at <https://github.com/giovanniscala/ErrorMitigation>.

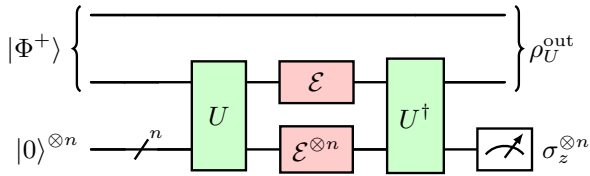


FIG. 6: Error filtration scheme: The reference and signal qubits are prepared in the maximally-entangled two-qubit state $|\Phi^+\rangle$. The signal qubit interacts with n ancillary qubits via the encoding unitary U , then passes through a noisy channel \mathcal{E} with (iid) errors. The inverse unitary followed by σ_z measurements on each ancilla decode the post-selected state ρ_U^{out} .

such cases, the analytical ansatz from Sec. III C are crucial for quickly identifying the best unitary U . For instance, in Quantum Key Distribution implementations, the key rate is often limited by phase modulator stabilizers [36, 52]. However, adopting a scheme like the one in Fig. 1 can avoid this limitation, at least not in every run. In this section, we specialize the scheme in Fig. 1 into Fig. 6. Here we quantify, under the action of the noisy channels, how well ρ_U^{out} preserves the entanglement of the initial state Φ^+ by computing the Entanglement fidelity $\mathcal{F}(\rho_U^{\text{out}}, \Psi^+)$. We denote the two qubits of the initial states with (R) the reference qubit that is not transmitted through the channel and with (S) the signal qubit that is affected by the noise, such that

$$|\Phi^+\rangle = \frac{1}{\sqrt{2}} (|0\rangle_R |0\rangle_S + |1\rangle_R |1\rangle_S). \quad (7)$$

At the output, the state ρ_U^{out} is conditioned on measuring the n ancillary qubits in the computational state $|0\rangle^{\otimes n}$. In fact, $\rho_U^{\text{out}} = \rho_{|0\rangle^{\otimes n}}^{\text{out}}/P_n$ represents the normalized density matrix obtained after post-selection, where P_n is the corresponding post-selection probability.

$$P_n = \text{Tr} \rho_{|0\rangle^{\otimes n}}^{\text{out}}. \quad (8)$$

The success probability P_n is independent of the cost function. However, in favour of readability, we always plot P_n alongside the cost function. The entanglement fidelity then reads

$$\mathcal{F}_n = \langle \Phi^+ | \rho_U^{\text{out}} | \Phi^+ \rangle. \quad (9)$$

The results of the numerical optimization are shown by the circle data points in Fig 7 and compared with the fidelity attainable without error reduction, which is $\mathcal{F}_0 = (1 + q_\varphi)/2$ for the dephasing channel, and $\mathcal{F}_0 = (1 + 3q_r)/4$ for the depolarizing channel (without error reduction this is achieved deterministically, i.e. with $P_0 = 1$). Figure 7 shows the trade-off arising when introducing ancillary qubits: with more ancillas the fidelity is enhanced but at the cost of reducing the success probability. We also note that the scheme works better for

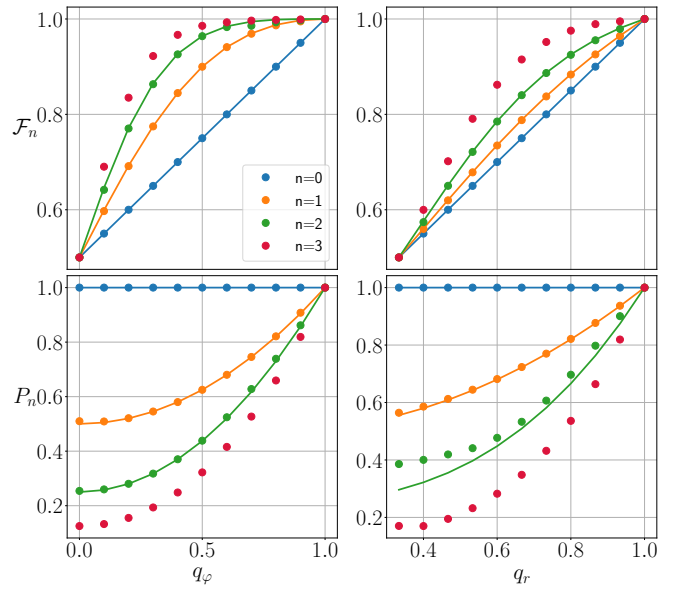


FIG. 7: Entanglement fidelity (upper panel) and success probability (lower panel) as functions of the noise parameters $q_\varphi \in [0, 1]$ for the *dephasing channel* (Eq. 2) and $q_r \in [1/3, 1]$ for the *depolarizing channel* (Eq. 5) with $n = 0, 1, 2, 3$ ancillae. Numerical results are shown as dots, and analytical results as solid lines in Eqs. (16)–(18 and (21)(24).

dephasing rather than depolarizing noise. This is in line with the observations of Refs. [28, 29] and corresponds to the fact that the depolarizing channel has higher Kraus rank (i.e., the number of Kraus operators) than the dephasing channel.

C. Ansätze for the optimal unitary

Here, we provide ansätze for the explicit form of the *optimal* unitary that matches the results of the numerical optimization concluding with our conjecture.

1. One ancilla

We note that, since the ancilla is initialized in $|0\rangle$, it is sufficient to consider the action of the encoding unitary on the states $|0\rangle_S |0\rangle_A$ and $|1\rangle_S |0\rangle_A$, where A labels the ancilla. Our ansatz for the optimal encoding follows directly from the optical error filtration scheme [17, 32]. We assume that the two states $|0\rangle_S |0\rangle_A$ and $|1\rangle_S |0\rangle_A$ are mapped into two Bell states, for example

$$|0\rangle_S |0\rangle_A \xrightarrow{U} U|0\rangle_S |0\rangle_A = \frac{|00\rangle + |11\rangle}{\sqrt{2}} = |\Phi^+\rangle_{SA}, \quad (10)$$

$$|1\rangle_S |0\rangle_A \xrightarrow{U} U|1\rangle_S |0\rangle_A = \frac{|10\rangle + |01\rangle}{\sqrt{2}} = |\Psi^+\rangle_{SA}. \quad (11)$$

This encoding can be implemented by different choices for the unitary U . For example, a possible choice is the one that maps the computation basis into the Bell basis. With this encoding rule, the initial state $|\Phi^+\rangle$ of reference and signal qubits in Eq. (7) is transformed as follows:

$$\begin{aligned} |\Phi^+\rangle_{RS}|0\rangle_A &= \frac{1}{\sqrt{2}} (|0\rangle_R|0\rangle_S|0\rangle_A + |1\rangle_R|1\rangle_S|0\rangle_A) \\ &\xrightarrow{U} \frac{1}{\sqrt{2}} (|0\rangle_R U|0\rangle_S|0\rangle_A + |1\rangle_R U|1\rangle_S|0\rangle_A) \\ &= \frac{1}{\sqrt{2}} (|0\rangle_R |\Phi^+\rangle_{SA} + |1\rangle_R |\Psi^+\rangle_{SA}) \\ &= \frac{1}{2} (|000\rangle + |011\rangle + |110\rangle + |101\rangle), \end{aligned} \quad (12)$$

where in the last line we have dropped the labels R, S, A .

Let us look in more detail to the case of dephasing channel. The action of this noise to each qubit can be described as the application of a random phase in the computation basis, expressed by the operator $e^{i\theta_j|1\rangle_j\langle 1|}$ applied on the j -th qubit, where θ_j is a random variable. Its probability density distribution $\mu(\theta)$ determines the dephasing parameter q_φ as

$$q_\varphi = \int d\theta \mu(\theta) \cos \theta. \quad (13)$$

The application of a random phase to the above state in Eq. (12) yields (recall that the reference is not subject to noise)

$$\frac{1}{2} (|000\rangle + e^{i\theta_1+i\theta_2}|011\rangle + e^{i\theta_1}|110\rangle + e^{i\theta_2}|101\rangle). \quad (14)$$

The application of the inverse circuit (mapping the Bell basis back into the computation basis), followed by the projection onto the state $|0\rangle$ of the ancilla, yields

$$|\psi_{\theta_1\theta_2}\rangle = \frac{1}{\sqrt{2}} \left(\frac{1 + e^{i\theta_1+i\theta_2}}{2} |00\rangle + \frac{e^{i\theta_1} + e^{i\theta_2}}{2} |11\rangle \right). \quad (15)$$

The above state is not normalized. To obtain the post-selection probability we need to average its squared modulus over the noise realizations, obtaining

$$P_1(q_\varphi) = \int d\theta_1 d\theta_2 \mu(\theta_1) \mu(\theta_2) \langle \psi_{\theta_1\theta_2} | \psi_{\theta_1\theta_2} \rangle = \frac{1 + q_\varphi^2}{2}. \quad (16)$$

Similarly, the entanglement fidelity reads

$$\begin{aligned} \mathcal{F}_1(q_\varphi) &= \frac{1}{P_1} \int d\theta_1 d\theta_2 \mu(\theta_1) \mu(\theta_2) |\langle \Phi^+ | \psi_{\theta_1\theta_2} \rangle|^2 \\ &= \frac{1}{2} + \frac{q_\varphi}{1 + q_\varphi^2}. \end{aligned} \quad (17)$$

The above values of the entanglement fidelity and the success probability match the numerical results up to machine precision, see Fig. 7. A similar construction

is presented in Appendix A for the case of depolarizing channel, yielding

$$P_1 = \frac{1 + q_r^2}{2}, \quad \mathcal{F}_1 = \frac{1 + 2q_r + 5q_r^2}{4(1 + q_r^2)}, \quad (18)$$

which also match the numerical results. In summary, for the case of one ancillary qubit, we formulate our conjecture for the optimal encoding:

Conjecture 1 *The optimal encoding unitary that maximizes the entanglement fidelity in the filtration scheme with one ancillary qubit maps the states of the input qubit into maximally entangled states as in Eqs. (10)–(11).*

2. Two ancillas

We now introduce an ansatz for the unitary in the case of two ancillas taking inspiration from the case of one ancilla. We note that, in a space of dimension four, an optimal encoding in the case of one ancilla was based on the equally weighted superposition of two vectors in the computational basis, see Eqs. (10),(11). We also note that these vectors have different parity. This suggests the following encoding rule with two ancillas:

$$\begin{aligned} |0\rangle_S |00\rangle_A &\xrightarrow{U} U|0\rangle_S |00\rangle_A \\ &= \frac{|000\rangle + |011\rangle + |101\rangle + |110\rangle}{2}, \end{aligned} \quad (19)$$

$$\begin{aligned} |1\rangle_S |00\rangle_A &\xrightarrow{U} U|1\rangle_S |00\rangle_A \\ &= \frac{|001\rangle + |010\rangle + |100\rangle + |111\rangle}{2}. \end{aligned} \quad (20)$$

In Appendix B, we compute the success probability and entanglement fidelity assuming this action of the unitary U . We obtain

$$P_2(q_\varphi) = \frac{1 + 3q_\varphi^2}{4} \quad \mathcal{F}_2(q_\varphi) = \frac{(q_\varphi + 1)^3}{6q_\varphi^2 + 2} \quad (21)$$

matching the numerical results in Fig. 7. For depolarizing noise, a similar encoding works, with some signs modified in the computational basis:

$$\begin{aligned} |0\rangle_S |00\rangle_A &\xrightarrow{U} U|0\rangle_S |00\rangle_A \\ &= \frac{|000\rangle + |011\rangle + |101\rangle + |110\rangle}{2}, \end{aligned} \quad (22)$$

$$\begin{aligned} |1\rangle_S |00\rangle_A &\xrightarrow{U} U|1\rangle_S |00\rangle_A \\ &= \frac{|001\rangle - |010\rangle + |100\rangle - |111\rangle}{2}. \end{aligned} \quad (23)$$

From this, we compute:

$$P_2 = \frac{1 + q_r^2 + 2q_r^3}{4}, \quad \mathcal{F}_2 = \frac{1 + 7q_r^2}{4(1 - q_r + 2q_r^2)}, \quad (24)$$

matching numerical results for depolarizing noise, as shown in Fig.7. We propose the following conjecture for optimal encoding with two ancillas:

Conjecture 2 *The optimal encoding unitary that maximizes the entanglement fidelity in the filtration scheme with two ancillary qubits maps the states of the input qubit into equally-weighted sums of computational states with given parity:*

$$|000\rangle \rightarrow \frac{|000\rangle + w_1|011\rangle + w_2|101\rangle + w_3|110\rangle}{2}, \quad (25)$$

$$|100\rangle \rightarrow \frac{|001\rangle + w_4|010\rangle + w_5|100\rangle + w_6|111\rangle}{2}, \quad (26)$$

where $|w_i|^2 = 1$.

This conjecture is verified not only for the entanglement fidelity, but also for some other figures of merit, as discussed in the following sections.

D. Noisy implementation of error filtration

In this Section, we look at what happens when the encoding procedure is imperfect.

In practical experiments, the introduction of ancillary qubits and the entangling unitary U inevitably adds noise into the system. One would expect that the impact of this *filtration-induced* noise may become more noticeable as we increase the number of ancillary qubits. However, here we show that there exists noise models for which this detrimental effect remains under control, and in fact, we can still obtain some benefits from increasing the number of ancillas.

We focus on two main sources of error: (i) ancillary qubits that may themselves be noisy, and (ii) cross-talk during encoding (U) and decoding (U^\dagger). The former is modeled by adding an extra depolarizing channel to each ancillary qubits, the latter by introducing stochastic swap of signal and ancillas each time a multi-qubit unitary is applied. Our goal is to see how these imperfections impact the entanglement fidelity of the protocol.

1. Noisy ancilla preparation

In this first scenario, we introduce a local depolarizing channel acting on each ancillary qubit, just before it enters the filtration circuit. The depolarizing channel is denoted \mathcal{D} and is characterized by a noise parameter q_a (see definition in Section II B). This models preparation noise of the initial ancillary qubits state. Even though we aim to protect the signal, errors on the ancillary qubits can still reduce the final fidelity. The scheme is depicted in Fig. (8). As more ancillae are added, the overall noise can grow, so it is important to see how well our method holds up in this situation.

To address this question, we perform the optimization of the fidelity in the presence of preparation noise. In the top panel of Fig. 10 we plot the computed optimal fidelity

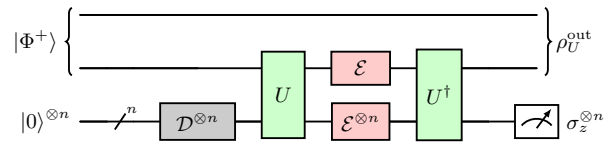


FIG. 8: Error filtration scheme with depolarizing noise in the preparation of the ancillary qubits: the signal qubit interacts with n noisy ancillary qubits before passing through the encoding unitary U , and then goes through the main noisy channel \mathcal{E} .

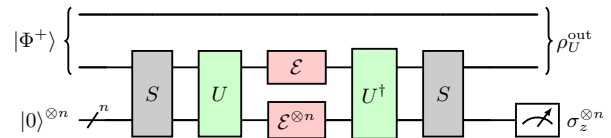


FIG. 9: Error filtration scheme with cross-talk between the signal and ancillary qubits: a random SWAP is applied between the signal qubit and ancillae at the encoding stage before U . The state then goes through the main channel \mathcal{E} and another random SWAP applies again after it is decoded by U^\dagger .

against the depolarizing parameter q_a applied to each ancilla qubit. When q_a approaches 1, the fidelity improves and moves closer to its ideal value. We observe that despite preparation noise, having more ancillary qubits still provides stronger suppression of errors.

2. Cross-talk

In the second scenario, we model unwanted cross-talk during the application of the encoding (U) and decoding (U^\dagger) multi-qubit unitary. The scheme is shown in Fig. (9). We model cross-talk during the encoding process by introducing random SWAP operations between the signal qubit and ancillae. We model this process as follows. In the case of $n = 1$ ancilla, with probability s no swap occurs and the encoding remains intact, and with probability $1 - s$ the signal qubit is swapped with the ancilla. In the case of $n = 2$ ancillae, the signal qubit can swap with either the first or second ancilla, each occurring with probability $\frac{1-s}{2}$. Likewise, for $n = 3$ ancillas, the individual swap probability is $\frac{1-s}{3}$.

We compute the optimized fidelity in the presence of this cross-talk mode. The results are shown in the bottom panel of Fig. 10 by varying the SWAP probability s , while keeping the main channel noise fixed. As s approaches 1 (ideal, no cross-talk limit), the fidelity gets its optimal value, and using more ancilla qubits further boosts performance. However, the filtration scheme shows some robustness to this noise model as increasing the number of ancillas systematically counteracts the effects of cross-talk, showing that our scheme remains robust despite noisy pre- and post-processing steps.

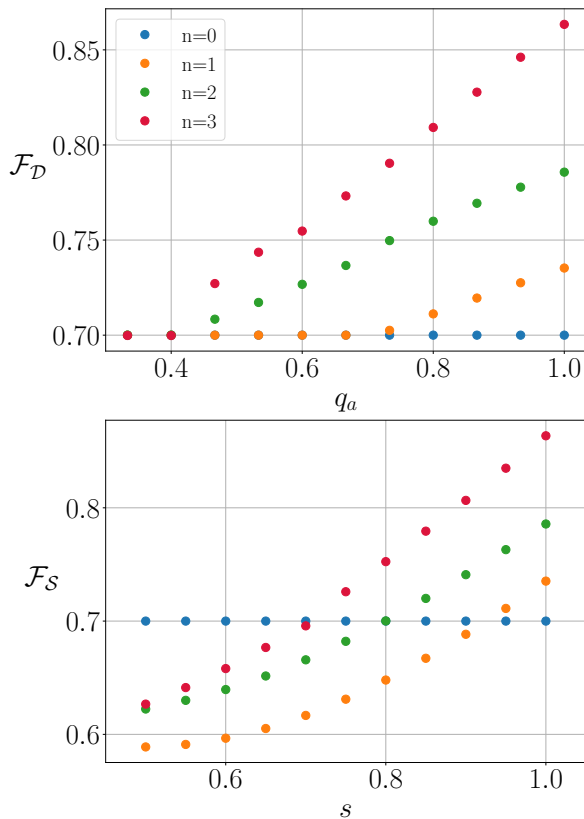


FIG. 10: Numerical results for the two error models described in Section III D. The top panel shows how the optimized entanglement fidelity \mathcal{F}_D depends on the preparation noise depolarizing parameter $q_a \in [\frac{1}{3}, 1]$, with the main channel noise fixed at $q_r = 0.7$. The bottom panel shows how the entanglement fidelity \mathcal{F}_S changes as functions of the swap probability $s \in [0.5, 1]$, again for a fixed channel noise strength of $q_r = 0.7$. Each curve corresponds to a different number of ancilla qubits ($n = 0, 1, 2, 3$).

E. Violation of Bell inequalities

The main challenge in implementing device-independent quantum key distribution [53–55] is reducing noise to violate suitable Bell inequalities. Therefore, we analyse whether our method is useful for this application. In a simple Bell scenario, a bipartite state ρ_{AB} of two qubits is shared between two distant labs, Alice (A) and Bob (B). In each lab, one of two possible observables is measured, represented by matrices $M_{i,j}$, where

$$M_{i,j} = \begin{pmatrix} \cos \theta_{ij} & e^{-i\phi_{ij}} \sin \theta_{ij} \\ e^{i\phi_{ij}} \sin \theta_{ij} & -\cos \theta_{ij} \end{pmatrix}. \quad (27)$$

Here $i = 0, 1$ labels the sub-systems ($i = 0$ for Alice and $i = 1$ for Bob), and $j = 0, 1$ labels two possible measurement settings. The measurements are dichotomic, i.e., each has two possible outcomes $a, b \in \{-1, +1\}$. After

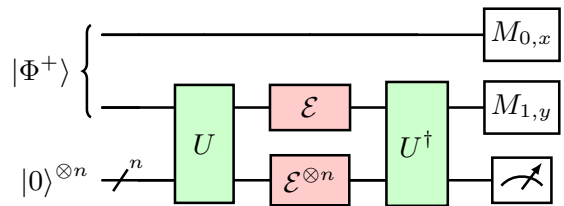


FIG. 11: Error filtration scheme designed to maximize CHSH inequality violation. A maximally-entangled two-qubit state $|\Phi^+\rangle$ is prepared in Alice’s lab, where she stores the first qubit without noise. The second qubit interacts with n ancillary qubits via the encoding unitary U and travels to Bob’s lab through a noisy channel \mathcal{E} . Bob applies the inverse unitary and measures the ancillary qubits in the computational basis. Alice and Bob perform the Bell test using local operators $M_{0,x}$ and $M_{0,y}$, conditioned on the ancillary qubits being in the state $|0\rangle^{\otimes n}$.

repeated measurements, Alice and Bob can estimate the CHSH functional [56]

$$\mathcal{B} = \left| \sum_{x,y=0}^1 (-1)^{xy} \text{Tr} (M_{0,x} \otimes M_{1,y} \rho_{AB}) \right|. \quad (28)$$

According to Bell’s theorem, a local realistic theory satisfies $\mathcal{B} \leq 2$. However, if ρ_{AB} is maximally entangled [57], this bound increases to $\mathcal{B} = 2\sqrt{2}$, allowing for secure communication provided $2 < \mathcal{B} \leq 2\sqrt{2}$. However, when ρ_{AB} is distributed between Alice and Bob, as in Fig. 11, noise in the communication line reduces the value of \mathcal{B} [58–63]. To counteract this, we apply our noise reduction technique to maintain secure communication by maximizing \mathcal{B} .

From Fig. 11, first, Alice locally prepares the entangled state $|\Phi^+\rangle$. Noise (either dephasing or depolarizing) is applied to the qubit transmitted to Bob, with error reduction aided by n ancillary qubits and an encoding/decoding unitary U . The ancillas interact with the signal qubit before the noisy channel, and both are subject to independent errors, followed by recombination using U^\dagger . By invoke the fair sampling assumption, the functional in Eq. (28) is computed on the normalized state $\rho_{AB} = \rho_{|0\rangle^{\otimes n}}^{\text{out}} / P_n$. This functional depends on parameters defining the unitary U (Section II) and the measurement settings θ_{ij} and ϕ_{ij} . We simulate two possible experimental scenarios: finding the optimal unitary for fixed θ_{ij} and ϕ_{ij} :

$$\beta_n^{\text{fix}} = \max_U \mathcal{B}_n, \quad (29)$$

and maximizing over both the unitary and measurement angles:

$$\beta_n^{\text{opt}} = \max_{U, \theta_{ij}, \phi_{ij}} \mathcal{B}_n. \quad (30)$$

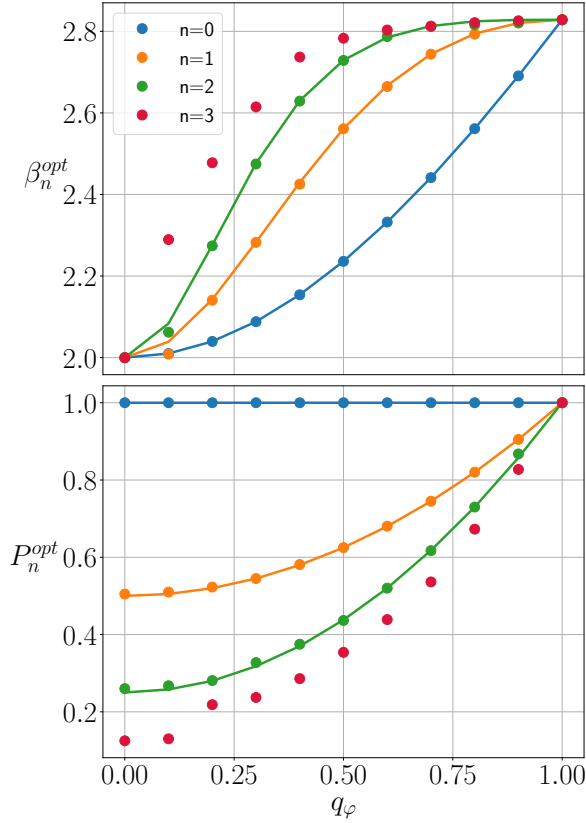


FIG. 12: Optimal CHSH value (top panel) optimizing also on the measurement settings (see Eq. (30)) and successful probability P_n (lower panels), plotted vs the noise parameter $q_\varphi \in [0.5, 1]$ for *dephasing channel*. Dots are for numerical optimization, solid lines for the ansatz unitary, for $n = 0, 1, 2, 3$ ancillary qubits.

For the estimation of β_n^{fix} we fix the values of θ_{ij}, ϕ_{ij} that maximize the CHSH functional with not error filtration applied (no ancilla). Given $|\Phi^+\rangle$, and for the depolarizing channel, these values are well-known:

$$\begin{aligned} (\phi_{0,0}, \theta_{0,0}) &= (0, 0), & (\phi_{0,1}, \theta_{0,1}) &= \left(0, \frac{\pi}{2}\right), \\ (\phi_{1,0}, \theta_{1,0}) &= \left(0, \frac{\pi}{4}\right), & (\phi_{1,1}, \theta_{1,1}) &= \left(\pi, \frac{\pi}{4}\right). \end{aligned} \quad (31)$$

Similarly, the optimal settings for dephasing noise with parameter q_φ are obtained for

$$\begin{aligned} (\phi_{0,0}, \theta_{0,0}) &= (0, 0), & (\phi_{0,1}, \theta_{0,1}) &= \left(0, \frac{\pi}{2}\right), \\ (\phi_{1,0}, \theta_{1,0}) &= (0, \arctan q_\varphi), & (\phi_{1,1}, \theta_{1,1}) &= (\pi, \arctan q_\varphi). \end{aligned} \quad (32)$$

Using these optimal settings, the maximum value of the Bell functional in the presence of dephasing and depolarizing noise, without our reduction scheme, are well-established [64]. They are given by:

$$\beta_0^{\text{fix}}(q_\varphi) = 2\sqrt{1 + q_\varphi^2}, \quad \beta_0^{\text{fix}}(q_r) = 2\sqrt{2} q_r. \quad (33)$$

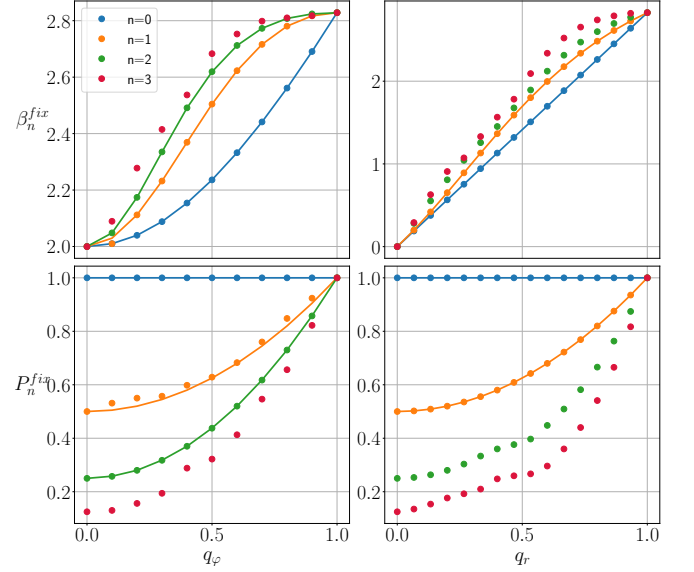


FIG. 13: CHSH value (upper panel) with fixed measurement settings and success probability (lower panel) as functions of the noise parameters $q_\varphi \in [0, 1]$ for the *dephasing channel* (Eq. (2)) and $q_r \in [1/3, 1]$ for the *depolarizing channel* (Eq. (5)) with $n = 0, 1, 2, 3$ ancillae. Numerical results are shown as dots, and analytical results as solid lines (Eqs. (16), (18), (21), (24),(34), (35)).

Based on the conjectures 1 and 2, we derive the following analytical expressions for the CHSH value after error filtration. For dephasing noise ($n = 1, 2$)

$$\beta_1^{\text{fix}}(q_\varphi) = \frac{6q_\varphi^2 + 2}{(q_\varphi^2 + 1)^{3/2}}, \quad \beta_2^{\text{fix}}(q_\varphi) = \frac{2(1 + 6q_\varphi^2 + q_\varphi^4)}{(1 + 3q_\varphi^2)\sqrt{1 + q_\varphi^2}}, \quad (34)$$

and for depolarizing noise ($n = 1$)

$$\beta_1^{\text{fix}}(q_r) = 2\sqrt{2} q_r \frac{1 + q_r}{1 + q_r^2}. \quad (35)$$

These are the solid lines shown in Fig. 13 that overlap with the numerical optimization, supporting the conjectures 1 and 2. The related success probability is in Eq. (18). However, we do not have a good ansatz in the case of the dephasing noise with $n = 3$ and depolarizing noise with $n = 2, 3$. It remains an open challenge to provide explicit analytical expressions in these cases.

Finally, the Bell functional in Eq. (30) includes also the optimization over measurement settings. In this case, the symmetry of the depolarizing noise implies that the optimal angles remain unchanged.

Instead, for the dephasing noise, optimizing over the angles improves the CHSH value, $\beta_n^{\text{opt}} > \beta_n^{\text{fix}}$. This is shown in Fig. 12, along with the matching values obtained our unitary encoding ansatz with one and two ancillae.

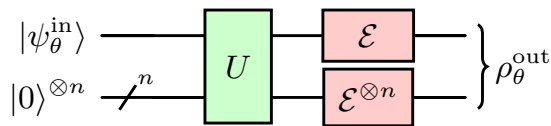


FIG. 14: Error filtration for parameter estimation. The signal qubit is initialized in $|\psi(\theta)\rangle = \cos(\theta/2)|0\rangle + \sin(\theta/2)|1\rangle$ (with θ the parameter to estimate) and, together with n ancillary qubits in $|0\rangle^{\otimes n}$, is encoded via U . The encoded state is then subjected to the local noisy channel \mathcal{E} . Post-selection on the ancillas is avoided (to retain full measurement counts), and the decoding unitary is omitted since QFI is invariant under unitary transformations.

F. Quantum metrology

In this section, we aim to improve the Quantum Fisher Information (QFI) of a qubit affected by depolarizing noise using our optimized error filtration technique. QFI is a key metric in quantum metrology, quantifying how much information a family of quantum states ρ_θ carries about a parameter θ (which may represent physical quantities like a phase shift or magnetic field strength) to be estimated. Formally, the QFI reads

$$Q = \text{Tr}(L^2 \rho_\theta), \quad (36)$$

where L is the symmetric logarithmic derivative [26, 65],

$$L = \sum_{l,m:p_l+p_m \neq 0} \frac{2 \langle e_m | \partial_\theta \rho | e_l \rangle}{\lambda_l + \lambda_m} |e_m\rangle \langle e_l|, \quad (37)$$

which is computed from the θ -dependent spectral decomposition

$$\rho_\theta = \sum_m \lambda_m |e_m\rangle \langle e_m|, \quad (38)$$

and depends on the derivative $\partial_\theta \rho$ of the density matrix with respect to the parameter θ .

The operational interpretation of the QFI is of particular interest in quantum metrology, as it quantifies the minimum statistical error attainable in the estimation of the parameter θ from M identical copies $\rho_\theta^{\otimes M}$. According to the quantum Cramér-Rao bound [26, 65], the statistical error $\Delta\theta$ is bounded from below as follows

$$\Delta\theta \geq (M Q)^{-1/2}. \quad (39)$$

The general scheme of Fig. 1 specializes as in Fig. 14 for the goal of parameter estimation. Additionally, since QFI is invariant under unitary transformations that are independent of θ , we may omit the decoding unitary U^\dagger . We also note that the QFI bounds the inverse of variance $\Delta\theta^2$ divided by the total number M of given independent copies of the state, and that post-selection on the ancillary qubits would artificially reduce the effective value

of M . Therefore, even if the post-selected QFI is augmented, this does not necessarily mean that the variance is made smaller. For this reason, as shown in Fig. 14, in this setup we do not post-select on the ancillary qubits (see also Ref. [32]).

As a case study we consider a standard phase estimation problem, where the parameter θ is initially encoded in the phase of a family of one-qubit pure states,

$$|\psi_\theta^{\text{in}}\rangle = e^{-i\theta\sigma_y/2}|0\rangle = \cos(\theta/2)|0\rangle + \sin(\theta/2)|1\rangle. \quad (40)$$

We briefly recall that if a state is measured without noise, the associated QFI is $Q = 1$. Under noise, however, the QFI decreases, reflecting greater uncertainty in estimating θ . For depolarizing noise with parameter q_r , the QFI of the output state $\rho_\theta = \mathcal{E}(|\psi_\theta^{\text{in}}\rangle\langle\psi_\theta^{\text{in}}|)$, returns $Q_0(q_r) = q_r^2$.

Interestingly, we obtained in Fig. 15 for $n = 1, 2, 3$ that our error reduction scheme improves the trend $Q_0(q_r) = q_r^2$. The QFI after error filtration is computed on the state ρ_θ^{out} including both signal and ancillas. For $n = 1$, applying the ansatz of conjecture 1 we are able to obtain the following value for the QFI,

$$Q_1(q_r) = \frac{2q_r^2}{q_r^2 + 1}, \quad (41)$$

which matches the numerical optimization. This is shown in Fig. 15. For $n = 2, 3$, only dotted lines are displayed in Fig. 15, leaving open the problem of finding an analytical expression for the optimized QFI. In conclusion we note that, for dephasing noise, the error-filtration scheme yields $Q = 1$ even without ancillas, as the phase shift θ around σ_y is unaffected by dephasing along σ_z . If dephasing occurs along σ_y , a one-qubit rotation mapping σ_y to σ_z restores $Q = 1$.

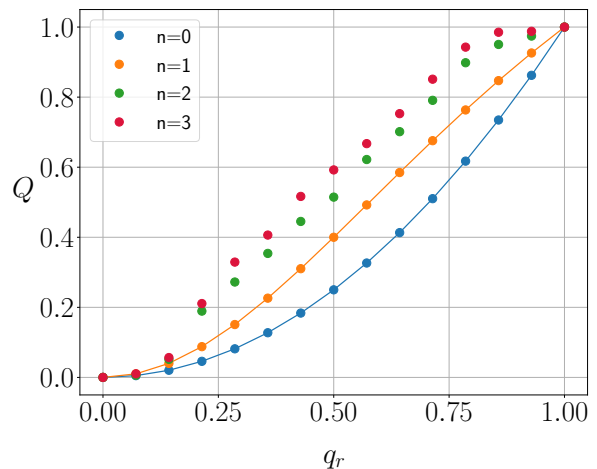


FIG. 15: The plot shows the optimal value of QFI after error filtration, following the optimization over all encoding unitary with $n = 0, 1, 2, 3$ ancillary qubits. The QFI is plotted vs the noise parameter of the depolarizing channel, see Eq. (4).

IV. COMPARISON WITH SUPERPOSED QUANTUM ERROR MITIGATION (SQEM)

We now compare our proposed optimized error filtration protocol to the recently introduced Superposed Quantum Error Mitigation (SQEM) scheme [28].

In Fig. 16, we compare the entanglement fidelity \mathcal{F}_n versus the dephasing noise parameter q_φ for three scenarios. The baseline case ($n = 0$) represents the circuit without any error mitigation (“no scheme”). The second scenario employs our error filtration protocol using a single ancilla ($n = 1$), while the third implements the SQEM protocol with one ancilla. In the figure, red markers denote SQEM results and orange markers represent our single-ancilla protocol. Notably, our approach consistently yields higher fidelity across the full noise range, surpassing SQEM at every tested value of q_φ .

These findings demonstrate that, under equivalent dephasing conditions, our error filtration scheme offers more robust protection of quantum information than SQEM. Overall, incorporating a single ancillary qubit as proposed significantly enhances fidelity—a critical advantage for near-term quantum devices, where hardware imperfections are unavoidable and robust error reduction is essential for scalable quantum computation.

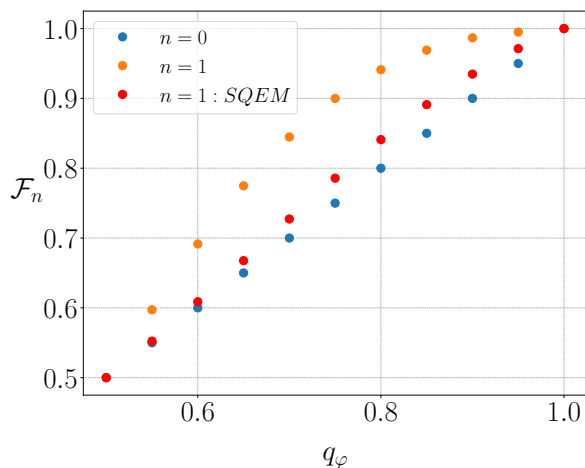


FIG. 16: Comparison of entanglement fidelity \mathcal{F}_n versus the dephasing noise parameter q_φ for different approaches: the baseline circuit ($n = 0$), our optimized error filtration protocol using one ancillary qubit, and the SQEM error mitigation scheme.

V. CONCLUSIONS

We studied *optimal* error filtration strategies for a signal qubit affected by depolarizing or dephasing noise. By assisting the signal qubit with one, two, and three ancilla

qubits, we find the optimal encoding parameters of the unitaries involved in our schemes. (i) In most cases the numerical results match with the analytical ansatz that we exposed in Conjectures 1 and 2, as depicted in all the figures where the points overlap the continuous line of the same colour. (ii) Our scheme yields non-trivial error filtration even with just one ancillary qubit. By contrast, previous schemes needed at least two assisting qubits to mitigate errors on a single qubit. (iii) We studied a more realistic scenario in comparison to previous works [28, 29], where the error reduction scheme was not robust to errors in the ancillary qubits. (iv) We developed an alternative approach to Ref. [66] to improve the entanglement fidelity, where it is referred to as *input-output fidelity*.

In addition, we examined scenarios where the encoding steps themselves could be imperfect, introducing ancillary qubit noise or cross-talk. Even under these conditions, our protocol showed resilience, with a clear advantage as the number of ancillary qubits increased. We also compared our proposal with the Superposed Quantum Error Mitigation (SQEM) scheme [28, 29], finding that our method provides consistently higher entanglement fidelities over a broad range of noise strengths. This comparative study underlines the robustness of our scheme, making it a promising candidate for near-term quantum devices.

Although our noise reduction scheme advances the state of the art, it has certain limitations that suggest future research directions. (i) The current approach is shown to be robust under certain realistic models of errors introduced by the scheme itself; this robustness analysis could be extended to more general noise models and put in relation to a suitable notion of fault-tolerance. (ii) Applications with few parameters are promising, but real-time hardware platforms require a dynamic analysis to optimize parameters rapidly [67, 68]. (iii) Combining our method with a quantum channel followed by its quasi-inversion could also be of significant interest [66]. (iv) Test the robustness of the method on multipartite Bell scenario for nonlocal quantum network [69–71].

ACKNOWLEDGMENTS

We thank D. Pomarico, for introducing us HTCondor, D. Amaro-Alcalá, F. Shahbeigi, R. Demkowicz-Dobrański, and E. Galvão for several clarifications. We are also grateful to S. P. Walborn, G. Lima and all their experimental quantum optics group of Universidad de Concepción for fruitful discussions. This work has received funding from the European Union — Next Generation EU, through PNRR MUR project CN00000013 ‘Italian National Centre on HPC, Big Data and Quantum Computing’, PNRR MUR project PE0000023-NQSTI ‘National Quantum Science and Technology Institute’, and INFN through the project “QUANTUM”.

- [1] C. L. Degen, F. Reinhard, and P. Cappellaro, *Reviews of modern physics* **89**, 035002 (2017).
- [2] A. N. Boto, P. Kok, D. S. Abrams, S. L. Braunstein, C. P. Williams, and J. P. Dowling, *Phys. Rev. Lett.* **85**, 2733 (2000).
- [3] J. P. Dowling, *Contemporary Physics* **49**, 125 (2008), <https://doi.org/10.1080/00107510802091298>.
- [4] D. Gottesman, T. Jennewein, and S. Croke, *Phys. Rev. Lett.* **109**, 070503 (2012).
- [5] F. V. Pepe, G. Scala, G. Chilleri, D. Triggiani, Y.-H. Kim, and V. Tamma, *The European Physical Journal Plus* **137**, 1 (2022).
- [6] M. Tsang, R. Nair, and X.-M. Lu, *Phys. Rev. X* **6**, 031033 (2016).
- [7] I. W. Primaatmaja, K. T. Goh, E. Y.-Z. Tan, J. T.-F. Khoo, S. Ghorai, and C. C.-W. Lim, *Quantum* **7**, 932 (2023).
- [8] V. Zapatero, T. van Leent, R. Arnon-Friedman, W.-Z. Liu, Q. Zhang, H. Weinfurter, and M. Curty, *npj Quantum Information* **9**, 10.1038/s41534-023-00684-x (2023).
- [9] J. Preskill, *Quantum* **2**, 79 (2018).
- [10] S. Endo, S. C. Benjamin, and Y. Li, *Physical Review X* **8**, 031027 (2018).
- [11] A. Strikis, D. Qin, Y. Chen, S. C. Benjamin, and Y. Li, *PRX Quantum* **2**, 040330 (2021).
- [12] Z. Cai, R. Babbush, S. C. Benjamin, S. Endo, W. J. Huggins, Y. Li, J. R. McClean, and T. E. O'Brien, *Reviews of Modern Physics* **95**, 045005 (2023).
- [13] S. Endo, Z. Cai, S. C. Benjamin, and X. Yuan, *Journal of the Physical Society of Japan* **90**, 032001 (2021).
- [14] Y. Suzuki, S. Endo, K. Fujii, and Y. Tokunaga, *PRX Quantum* **3**, 010345 (2022).
- [15] G. Acampora, M. Grossi, and A. Vitiello, in *2021 IEEE congress on evolutionary computation (CEC)* (IEEE, 2021) pp. 1826–1832.
- [16] M. Lostaglio and A. Ciani, *Physical review letters* **127**, 200506 (2021).
- [17] N. Gisin, N. Linden, S. Massar, and S. Popescu, *Phys. Rev. A* **72**, 012338 (2005).
- [18] M. Steffen, Differences in error suppression, mitigation, and correction, <https://www.ibm.com/quantum/blog/quantum-error-suppression-mitigation-correction> (2022), IBM Quantum Blog.
- [19] L.-P. Lamoureaux, E. Brainis, N. J. Cerf, P. Emplit, M. Haelterman, and S. Massar, *Phys. Rev. Lett.* **94**, 230501 (2005).
- [20] M. A. Nielsen and I. L. Chuang, *Quantum computation and quantum information* (Cambridge university press, 2010).
- [21] N. Brunner, D. Cavalcanti, S. Pironio, V. Scarani, and S. Wehner, *Reviews of Modern Physics* **86**, 419 (2014).
- [22] V. Scarani, *Bell Nonlocality* (Oxford University Press, 2019).
- [23] F. Xu, X. Ma, Q. Zhang, H.-K. Lo, and J.-W. Pan, *Reviews of Modern Physics* **92**, 10.1103/revmodphys.92.025002 (2020).
- [24] C. Portmann and R. Renner, *Reviews of Modern Physics* **94**, 025008 (2022).
- [25] N. Gigena, E. Panwar, G. Scala, M. Araújo, M. Farkas, and A. Chaturvedi, arXiv preprint arXiv:2405.08743 (2024).
- [26] J. S. Sidhu and P. Kok, *AVS Quantum Science* **2**, 014701 (2020), https://pubs.aip.org/avs/aqs/article-pdf/doi/10.1116/1.5119961/16700179/014701_1_online.pdf.
- [27] I. Cong, S. Choi, and M. D. Lukin, *Nature Physics* **15**, 1273–1278 (2019).
- [28] J. Miguel-Ramiro, Z. Shi, L. Dellantonio, A. Chan, C. A. Muschik, and W. Dür, *Phys. Rev. Lett.* **131**, 230601 (2023).
- [29] J. Miguel-Ramiro, Z. Shi, L. Dellantonio, A. Chan, C. A. Muschik, and W. Dür, *Phys. Rev. A* **108**, 062604 (2023).
- [30] G. Lee, C. T. Hann, S. Puri, S. Girvin, and L. Jiang, *Physical Review Letters* **131**, 190601 (2023).
- [31] M. K. Vijayan, A. P. Lund, and P. P. Rohde, *Quantum* **4**, 303 (2020).
- [32] Z. Huang and C. Lupo, *Phys. Rev. A* **110**, 052431 (2024).
- [33] H. Karthik, S. Gómez, F. Quinteros, M. Pawłowski, S. Walborn, G. Lima, E. Gómez, *et al.*, arXiv preprint arXiv:2411.07924 (2024).
- [34] S. Stein, S. Xu, A. W. Cross, T. J. Yoder, A. Javadi-Abhari, C. Liu, K. Liu, Z. Zhou, C. Guinn, Y. Ding, Y. Ding, and A. Li, arXiv preprint arXiv:2411.03202 (2024).
- [35] D. Pérez Castro, J. Fernández-Herrerín, A. Fernández-Vilas, M. Fernández-Veiga, and R. P. Díaz Redondo, *Elsevier BV* 10.2139/ssrn.5093821 (2025).
- [36] S. Rojas-Rojas, D. Martínez, K. Sawada, L. Pereira, S. P. Walborn, E. S. Gómez, N. K. Bernardes, and G. Lima, *Quantum* **8**, 1436 (2024).
- [37] D. Martínez, E. S. Gómez, J. Cariñe, L. Pereira, A. Delgado, S. P. Walborn, A. Tavakoli, and G. Lima, *Nature Physics* 10.1038/s41567-022-01845-z (2022).
- [38] S. Rojas-Rojas, G. C. nas, G. Saavedra, E. S. Gómez, S. P. Walborn, and G. Lima, *Opt. Express* **29**, 23381 (2021).
- [39] V. V. Shende, I. L. Markov, and S. S. Bullock, *Physical Review A* **69**, 062321 (2004).
- [40] M. Möttönen and J. J. Vartiainen, *Trends in Quantum Computing Research* , 149 (2006).
- [41] F. S. Khan and M. Perkowski, arXiv preprint quant-ph/0511041 (2005).
- [42] A. M. Krol, A. Sarkar, I. Ashraf, Z. Al-Ars, and K. Bertels, *Applied Sciences* **12**, 759 (2022).
- [43] A. Barenco, C. H. Bennett, R. Cleve, D. P. DiVincenzo, N. Margolus, P. Shor, T. Sleator, J. A. Smolin, and H. Weinfurter, *Physical review A* **52**, 3457 (1995).
- [44] S. Bullock and I. Markov, *Phys. Rev. A* **68**, 012318 (2003).
- [45] G. Cybenko, *Computing in science & engineering* **3**, 27 (2001).
- [46] M. Möttönen, J. J. Vartiainen, V. Bergholm, and M. M. Salomaa, *Physical review letters* **93**, 130502 (2004).
- [47] C. C. Paige and M. Wei, *Linear Algebra and its Applications* **208**, 303 (1994).
- [48] J. J. Vartiainen, M. Möttönen, and M. M. Salomaa, *Physical review letters* **92**, 177902 (2004).
- [49] R. Wiersema, D. Lewis, D. Wierichs, J. Carrasquilla, and N. Killoran, *Quantum* **8**, 1275 (2024).
- [50] V. V. Shende, S. S. Bullock, and I. L. Markov, *Proceedings of the 2005 Asia and South Pacific Design Automation Conference ASP-DAC '05*, 272–275 (2005).
- [51] INFN Bari, High Performance Computing (HPC)

- Cluster at ReCaS-Bari, <https://www.recas-bari.it/index.php/it/>, dedicated HPC cluster with 8000 cores and NVIDIA K40 accelerators.
- [52] J. Cariñe, G. Cañas, P. Skrzypczyk, I. Šupić, N. Guerrero, T. Garcia, L. Pereira, M. A. S. Prosser, G. B. Xavier, A. Delgado, S. P. Walborn, D. Cavalcanti, and G. Lima, *Optica* **7**, 542 (2020).
- [53] D. P. Nadlinger, P. Drmota, B. C. Nichol, G. Araneda, D. Main, R. Srinivas, D. M. Lucas, C. J. Ballance, K. Ivanov, E. Y.-Z. Tan, P. Sekatski, R. L. Urbanke, R. Renner, N. Sangouard, and J.-D. Bancal, *Nature* **607**, 682 (2022).
- [54] W.-Z. Liu, Y.-Z. Zhang, Y.-Z. Zhen, M.-H. Li, Y. Liu, J. Fan, F. Xu, Q. Zhang, and J.-W. Pan, *Physical Review Letters* **129**, 050502 (2022).
- [55] W. Zhang, T. van Leent, K. Redeker, R. Garthoff, R. Schwonnek, F. Fertig, S. Eppelt, W. Rosenfeld, V. Scarani, C. C.-W. Lim, and H. Weinfurter, *Nature* **607**, 687 (2022).
- [56] J. F. Clauser, M. A. Horne, A. Shimony, and R. A. Holt, *Physical Review Letters* **23**, 880 (1969).
- [57] B. S. Cirel'son, *Letters in Mathematical Physics* **4**, 93 (1980).
- [58] C. Abellán and B. B. T. Collaboration, *Nature* **557**, 212 (2018), arXiv:1805.04431 [quant-ph].
- [59] N. Gigena, G. Scala, and A. Mandarino, *International Journal of Quantum Information* 10.1142/s0219749923400051 (2022).
- [60] J. Handsteiner, A. S. Friedman, D. Rauch, J. Gallicchio, B. Liu, H. Hosp, J. Kofler, D. Bricher, M. Fink, C. Leung, A. Mark, H. T. Nguyen, I. Sanders, F. Steinlechner, R. Ursin, S. Wengerowsky, A. H. Guth, D. I. Kaiser, T. Scheidl, and A. Zeilinger, *Physical Review Letters* **118**, 10.1103/physrevlett.118.060401 (2017).
- [61] D. Rauch, J. Handsteiner, A. Hochrainer, J. Gallicchio, A. S. Friedman, C. Leung, B. Liu, L. Bulla, S. Ecker, F. Steinlechner, R. Ursin, B. Hu, D. Leon, C. Benn, A. Ghedina, M. Cecconi, A. H. Guth, D. I. Kaiser, T. Scheidl, and A. Zeilinger, *Phys. Rev. Lett.* **121**, 080403 (2018).
- [62] T. Scheidl, R. Ursin, J. Kofler, S. Ramelow, X.-S. Ma, T. Herbst, L. Ratschbacher, A. Fedrizzi, N. K. Langford, T. Jennewein, and A. Zeilinger, *Proceedings of the National Academy of Sciences (USA)* **107**, 19708 (2010), arXiv:0811.3129 [quant-ph].
- [63] D. Aktas, S. Tanzilli, A. Martin, G. Pütz, R. Thew, and N. Gisin, *Physical Review Letters* **114**, 220404 (2015), arXiv:1504.08332 [quant-ph].
- [64] R. Horodecki, P. Horodecki, and M. Horodecki, *Physics Letters A* **200**, 340 (1995).
- [65] M. G. Paris, *International Journal of Quantum Information* **7**, 125 (2009).
- [66] F. Shahbeigi, K. Sadri, M. Moradi, K. Życzkowski, and V. Karimipour, *Journal of Physics A: Mathematical and Theoretical* **54**, 345301 (2021).
- [67] R. Renner, *International Journal of Quantum Information* **6**, 1 (2008).
- [68] J. Kelly, R. Barends, A. G. Fowler, A. Megrant, E. Jeffrey, T. C. White, D. Sank, J. Y. Mutus, B. Campbell, Y. Chen, *et al.*, *Nature* **519**, 66 (2015).
- [69] D. Paneru, F. D. Colandrea, A. D'Errico, and E. Karimi, arXiv preprint quant-ph/2412.09768 (2024).
- [70] M. Karczewski, G. Scala, A. Mandarino, A. B. Sainz, and M. Żukowski, *Journal of Physics A: Mathematical and Theoretical* **55**, 384011 (2022).
- [71] S. Boreiri, N. Brunner, and P. Sekatski, arXiv preprint quant-ph/2501.14027 (2025).

Appendix A: Ansatz for the encoding unitary with one ancilla

Consider the following encoding unitary, which maps the computational basis into the Bell basis:

$$U = \sum_{j,k=0,1} |\Phi_{jk}\rangle\langle jk|, \quad (\text{A1})$$

where Φ_{jk} denote the Bell states. The inverse unitary is

$$U^\dagger = \sum_{j,k=0,1} |jk\rangle\langle\Phi_{jk}|. \quad (\text{A2})$$

To compute the entanglement fidelity, we start with the state (with ancilla initialized in $|0\rangle$)

$$\frac{1}{\sqrt{2}} (|0\rangle_R|0\rangle_S|0\rangle_A + |1\rangle_R|1\rangle_S|0\rangle_A). \quad (\text{A3})$$

Applying the encoding unitary to this state we obtain

$$\xrightarrow{U} \frac{1}{\sqrt{2}} (|0\rangle_R|\Phi_{00}\rangle_{SA} + |1\rangle_R|\Phi_{10}\rangle_{SA}). \quad (\text{A4})$$

If the local noise is described as a Pauli channel, then it can be viewed as the application of random Pauli unitaries. Let V_1 be the Pauli unitary applied on qubit S and V_2 the one applied on qubit A . For a given realization of the noise, the above state becomes

$$\frac{1}{\sqrt{2}} (|0\rangle_R(V_1 \otimes V_2)|\Phi_{00}\rangle_{SA} + |1\rangle_R(V_1 \otimes V_2)|\Phi_{10}\rangle_{SA}). \quad (\text{A5})$$

After the noise is applied, it is time to apply the inverse unitary, yielding

$$\begin{aligned} \xrightarrow{U^\dagger} \sum_{jk} \frac{1}{\sqrt{2}} (|0\rangle_R|jk\rangle\langle\Phi_{jk}|(V_1 \otimes V_2)|\Phi_{00}\rangle_{SA} \\ + |1\rangle_R|jk\rangle\langle\Phi_{jk}|(V_1 \otimes V_2)|\Phi_{10}\rangle_{SA}). \end{aligned} \quad (\text{A6})$$

Since we post-selected on the ancillary qubit being in the state $|0\rangle$, of the above state we only need to consider the terms with $k = 0$. The resulting, non-normalized state is

$$\begin{aligned} |\psi_{V_1, V_2}\rangle = \frac{1}{\sqrt{2}} \sum_j |0\rangle_R|j\rangle\langle\Phi_{j0}|(V_1 \otimes V_2)|\Phi_{00}\rangle_{SA} \\ + |1\rangle_R|j\rangle\langle\Phi_{j0}|(V_1 \otimes V_2)|\Phi_{10}\rangle_{SA}. \end{aligned} \quad (\text{A7})$$

From this we obtain the success probability after averaging the quantity $\langle|\psi_{V_1, V_2}\rangle\langle\psi_{V_1, V_2}|$ over the random Pauli unitaries:

$$\begin{aligned}
P_1 &= \frac{1}{2} \sum_{V_1, V_2} \pi(V_1)\pi(V_2) \sum_j \left(|\langle \Phi_{j0} | V_1 \otimes V_2 | \Phi_{00} \rangle|^2 |\langle \Phi_{j0} | V_1 \otimes V_2 | \Phi_{10} \rangle|^2 \right) \\
&= \frac{1}{2} \sum_{V_1, V_2} \pi(V_1)\pi(V_2) \left(|\langle \Phi_{00} | V_1 \otimes V_2 | \Phi_{00} \rangle|^2 + |\langle \Phi_{10} | V_1 \otimes V_2 | \Phi_{00} \rangle|^2 + |\langle \Phi_{00} | V_1 \otimes V_2 | \Phi_{10} \rangle|^2 + |\langle \Phi_{10} | V_1 \otimes V_2 | \Phi_{10} \rangle|^2 \right),
\end{aligned} \tag{A8}$$

where $\pi(V)$ is the probability of the Pauli unitary V . For the case of depolarizing channel, the three Pauli errors have the same probability, equal to $(1 - p_r)/3$. This symmetry implies

$$\begin{aligned}
P_1(q_r) &= \sum_{V_1, V_2} \pi(V_1)\pi(V_2) \left(|\langle \Phi_{00} | V_1 \otimes V_2 | \Phi_{00} \rangle|^2 + |\langle \Phi_{10} | V_1 \otimes V_2 | \Phi_{00} \rangle|^2 \right) \\
&= p_r^2 + \frac{(1 - p_r)^2}{3} + 2p_r \frac{1 - p_r}{3} + 2 \frac{(1 - p_r)^2}{9} \\
&= \frac{5 - 4p_r + 8p_r^2}{9} = \frac{1 + q_r^2}{2}.
\end{aligned} \tag{A9}$$

The un-normalized fidelity is obtained by taking the average of the quantity $|\langle \Phi^+ | \psi_{V_1, V_2} \rangle|^2$,

$$\sum_{V_1, V_2} \pi(V_1)\pi(V_2) |\langle \Phi^+ | \psi \rangle|^2 = \frac{1}{4} \sum_{V_1, V_2} \pi(V_1)\pi(V_2) |\langle \Phi_{00} | V_1 \otimes V_2 | \Phi_{00} \rangle + \langle \Phi_{10} | V_1 \otimes V_2 | \Phi_{10} \rangle|^2. \tag{A10}$$

Note that each term $\langle \Phi_{00} | V_1 \otimes V_2 | \Phi_{00} \rangle$ and $\langle \Phi_{10} | V_1 \otimes V_2 | \Phi_{10} \rangle$ is non-zero only if $V_1 = V_2$. Therefore, the non-normalized fidelity reads

$$\frac{1}{4} \sum_V \pi(V)^2 |\langle \Phi_{00} | V \otimes V | \Phi_{00} \rangle + \langle \Phi_{10} | V \otimes V | \Phi_{10} \rangle|^2. \tag{A11}$$

Also note $\langle \Phi_{00} | V \otimes V | \Phi_{00} \rangle = \pm 1$ as well as $\langle \Phi_{10} | V \otimes V | \Phi_{10} \rangle = \pm 1$, but they have the same sign only if $V = \sigma_0$ or $V = \sigma_y$ ². Finally we obtain the following value for the non-normalized fidelity:

$$\sum_{V=\sigma_0, \sigma_2} p(V)^2 = p_r^2 + \left(\frac{1 - p_r}{3} \right)^2 = \frac{1 + 2q_r + 5q_r^2}{8}. \tag{A12}$$

Computing the (normalized) fidelity we obtain the result presented in Eq. (18),

$$\mathcal{F}_1(q_r) = \frac{1}{4} \frac{1 + 2q_r + 5q_r^2}{1 + q_r^2}. \tag{A13}$$

Appendix B: Ansatz for the encoding unitary with two ancillas

The encoding rule in Eqs. (19)-(20) can be obtained from different choices of the encoding unitary U . One possible choice is a unitary that is isomorphic to the direct sum of two four-dimensional quantum Fourier transform. In the three-qubit computational basis $\{|0\rangle_S|00\rangle_A, |0\rangle_S|01\rangle_A, |0\rangle_S|10\rangle_A, |0\rangle_S|11\rangle_A, |1\rangle_S|00\rangle_A, |1\rangle_S|01\rangle_A, |1\rangle_S|10\rangle_A, |1\rangle_S|11\rangle_A\}$, this is represented by the unitary matrix

$$U = \frac{1}{2} \left(\begin{array}{cccc|cccc}
1 & 0 & 0 & 1 & 0 & 1 & 1 & 0 \\
0 & 1 & -1 & 0 & 1 & 0 & 0 & -1 \\
0 & 1 & -i & 0 & -1 & 0 & 0 & i \\
1 & 0 & 0 & i & 0 & -1 & -i & 0 \\
\hline
0 & 1 & 1 & 0 & 1 & 0 & 0 & 1 \\
1 & 0 & 0 & -1 & 0 & 1 & -1 & 0 \\
1 & 0 & 0 & -i & 0 & -1 & i & 0 \\
0 & 1 & i & 0 & -1 & 0 & 0 & -i
\end{array} \right). \tag{B1}$$

² The Pauli unitary here is σ_2 because of our choice of the encoding into Bell states. For a different we may have a different Pauli

error, but only one Pauli error can yield the same sign on both the terms.

Note that this matrix implements a quantum Fourier transform in each subspace of given parity.

Let us consider the application of this encoding rule to mitigate dephasing noise. We start from the entangled state $|\Phi^+\rangle$ between reference and system qubit, then apply the encoding unitary to the system and ancillary qubits:

$$|\Phi^+\rangle_{RS}|00\rangle_A = \frac{1}{\sqrt{2}} (|00\rangle_{RS}|00\rangle_A + |11\rangle_{RS}|00\rangle_A) \quad (\text{B2})$$

$$\xrightarrow{U} \frac{1}{\sqrt{2}} \left(|0\rangle_R \frac{|000\rangle + |011\rangle + |101\rangle + |110\rangle}{2} + |1\rangle_R \frac{|001\rangle + |010\rangle + |100\rangle + |111\rangle}{2} \right). \quad (\text{B3})$$

As done in Section III C we apply a local random phase to each qubit (except the reference). A given realization of the noise yields

$$\frac{1}{\sqrt{2}} \left(|0\rangle_R \frac{|000\rangle + e^{i\theta_2+i\theta_3}|011\rangle + e^{i\theta_1+i\theta_3}|101\rangle + e^{i\theta_1+i\theta_2}|110\rangle}{2} + |1\rangle_R \frac{e^{i\theta_3}|001\rangle + e^{i\theta_2}|010\rangle + e^{i\theta_1}|100\rangle + e^{i\theta_1+i\theta_2+i\theta_3}|111\rangle}{2} \right). \quad (\text{B4})$$

Applying the inverse unitary and after post-selection on the ancillary qubit, we obtain the non-normalized state

$$|\psi_{\theta_1, \theta_2, \theta_3, \theta_4}\rangle = \frac{1}{\sqrt{2}} \left(|0\rangle_R |0\rangle_S \frac{1 + e^{i\theta_2+i\theta_3} + e^{i\theta_1+i\theta_3} + e^{i\theta_1+i\theta_2}}{4} + |1\rangle_R |1\rangle_S \frac{e^{i\theta_3} + e^{i\theta_2} + e^{i\theta_1} + e^{i\theta_1+i\theta_2+i\theta_3}}{2} \right). \quad (\text{B5})$$

First, the probability of successful post-selection is obtained from the average over noise realizations of

$$|\langle \psi_{\theta_1, \theta_2, \theta_3, \theta_4} | \psi_{\theta_1, \theta_2, \theta_3, \theta_4} \rangle|^2 = \frac{1}{2} \left| \frac{1 + e^{i\theta_2+i\theta_3} + e^{i\theta_1+i\theta_3} + e^{i\theta_1+i\theta_2}}{4} \right|^2 + \frac{1}{2} \left| \frac{e^{i\theta_3} + e^{i\theta_2} + e^{i\theta_1} + e^{i\theta_1+i\theta_2+i\theta_3}}{4} \right|^2. \quad (\text{B6})$$

From this we obtain

$$P_2(q_\varphi) = \frac{1 + 3q_\varphi^2}{4}. \quad (\text{B7})$$

Second, the non-normalized entanglement fidelity is obtained from the average over noise realization of

$$|\langle \Phi^+ | \psi_{\theta_1, \theta_2, \theta_3, \theta_4} \rangle|^2 = \left| \frac{e^{i\theta_3} + e^{i\theta_2} + e^{i\theta_1} + e^{i\theta_1+i\theta_2+i\theta_3} + e^{i\theta_3} + e^{i\theta_2} + e^{i\theta_1} + e^{i\theta_1+i\theta_2+i\theta_3}}{8} \right|^2. \quad (\text{B8})$$

From this we obtain the non-normalized fidelity

$$\left(\frac{1 + q_\varphi}{2} \right)^3. \quad (\text{B9})$$

Intuitively, a good encoding rule is such that the probability of success P_2 is minimized and the quantity non-normalized fidelity $P_2 \mathcal{F}_2$ is maximized. With the above choice we obtain

$$\mathcal{F}_2(q_\varphi) = \frac{(q_\varphi + 1)^3}{6q_\varphi^2 + 2}. \quad (\text{B10})$$
